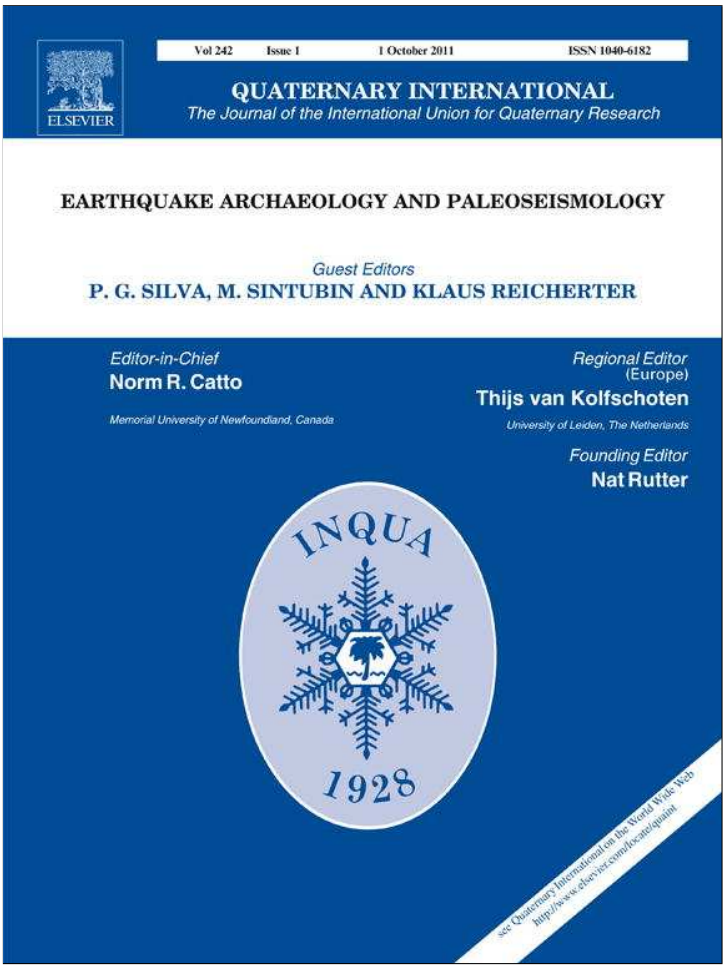

Quaternary International 242 (2011) 201–212

Contents lists available at ScienceDirect

Quaternary International

journal homepage: www.elsevier.com/locate/quaint

# Geomarkers of the 218–209 BC Atlantic tsunami in the Roman *Lacus Ligustinus* (SW Spain): A palaeogeographical approach

Joaquín Rodríguez-Vidal [a,*], Francisco Ruiz [a], Luis M. Cáceres [a], Manuel Abad [a], María Luz González-Regalado [a], Manuel Pozo [b], María I. Carretero [c], Antonio M. Monge Soares [d], Francisco Gómez Toscano [e]

[a] Departamento de Geodinámica y Paleontología, Universidad de Huelva, Avda. Tres de Marzo, s/n, 21071 Huelva, Spain
[b] Departamento de Geología y Geoquímica, Universidad Autónoma de Madrid, 28049 Madrid, Spain
[c] Departamento de Cristalografía, Mineralogía y Química Agrícola, Universidad de Sevilla, Apdo. 553, 41071 Sevilla, Spain
[d] Radiocarbon Dating Laboratory, Instituto Tecnológico e Nuclear, Estrada Nacional 10, 2686-953 Sacavém, Portugal
[e] Departamento de Historia I, Universidad de Huelva, Avda. Tres de Marzo, s/n, 21071 Huelva, Spain

ARTICLE INFO

*Article history:*
Available online 3 February 2011

ABSTRACT

Between 218 and 209 BC, the western coasts of Iberia suffered the impact of a historical tsunami, with an epicentre probably located in the Atlantic Ocean near the Cape St. Vincent area (SW Portugal). Palaeogeographical changes in the River Guadalquivir estuary, the ancient Roman *Lacus Ligustinus*, have been recorded in erosional and depositional landforms, both stratigraphically and as landscape relicts. The tsunamigenic waves (run-up of ~5 m) and their subsequent backwash eroded the previous littoral spits transversally, generating rectilinear cliffs and incisions. The littoral foredunes were also eroded and reactivated as transgressive dunes over the edge of the marshes. Former coastal sediments (~520–100 BC) generated overwash deposits, ebb tide deltas and sand sheets within the estuary, as well as a subsequent bioclastic beach on the lagoon shore, defining the post-tsunami (130 BC–80 AD) estuarine shoreline (Roman lagoon). Some coastal pre-Roman (7th to 3rd centuries BC) human settlements were abandoned, and later, in the Roman period (1st century AD), saltworks were installed. Morphological and sedimentological changes in the coast triggered by this event were similar or greater than the changes in coastal features related to the AD 1755 Lisbon tsunami.



## 1. Introduction

The study of tsunami has undergone rapid and dramatic development in recent years, and the associated literature has grown exponentially, with a variety of investigative approaches being presented. The papers used in this study represent selective aspects that have been particularly useful, but they are not representative of the entire spectrum of approaches to the problem.

Great tsunami have tremendous morphological effects and drastic ecological impacts in coastal areas (Borrero, 2005). The morphological changes caused to the coasts of Thailand and Indonesia by deposits from the December 26, 2004 tsunami (Fagherazzi and Du, 2008) provide a case-study for the interpretation of coastal sedimentation associated with large tsunami and their recurrence (Monecke et al., 2008).

The Holocene geological record of littoral areas has received increasing attention in recent years. The multidisciplinary analysis of cores collected in estuaries, lagoons, salt marshes or deltas has revealed broad information about the evolution of these environments, global or regional sea-level changes, palaeoclimatology, and the effects of anthropogenic actions during this period (Borrego et al., 2004; Vilanova et al., 2006; Selby and Smith, 2007). In this context, mineralogical composition and geochemistry is an important tool to infer the origin of sediments, the variations of some physical–chemical water parameters, and palaeoenvironments (Chamley, 1989; Carretero et al., 2002; Mackie et al., 2007).

This record may include distinctive sedimentary layers that have been attributed to storms, cyclones, hurricanes or tsunami. These high-energy events cause the deposition of sedimentary beds with characteristic textural and mineralogical features (Clague et al., 2000; Singarasubramanian et al., 2006; Babu et al., 2007).

The southwestern Spanish coast is a low-probability tsunamigenic area (Galbis, 1932; Reicherter, 2001). Although sixteen tsunami are documented for the time-period between 218 BC and

* Corresponding author. Fax: +34959219440.
*E-mail address:* jrvidal@uhu.es (J. Rodríguez-Vidal).

1040-6182/$ – see front matter © 2011 Elsevier Ltd and INQUA. All rights reserved.
doi:10.1016/j.quaint.2011.01.032

AD 1900 (Campos, 1991), there are still few papers focused on their geological record (e.g., Luque et al., 2001, 2002; Ruiz et al., 2004, 2005; Scheffers and Kelletat, 2005; Pozo et al., 2010).

The great Lisbon earthquake and tsunami of AD 1755 is the more recent one recorded on the coasts of southern Iberia, NW Morocco and the Atlantic islands. The earthquake MSK intensity can be estimated at VIII–IX in the Huelva-Cádiz sector, and its moment magnitude $M_w$ 8.7 (Baptista et al., 1998), recently re-evaluated as $M_w$ 8.5 ± 0.3 (Solares and Arroyo, 2004). The highest tsunami run-up recorded in the Azores Islands and along the SW Portuguese mainland shore was 10–15 m, corresponding to an event intensity of IV–V (large–very large) according to Alexander (1993) and VII–VIII (damaging–heavily damaging) on the Papadopoulos–Imamura scale. Recent investigations in the towns of Cádiz (Blanc, 2008) and Huelva (Lima et al., 2010) show a very probable run-up of 4–5 m above present m.s.l.

The main objective of this paper is to document the geological markers left by the historically documented tsunami of 218–209 BC within the ancient Roman *Lacus Ligustinus* (Guadalquivir estuary, Fig. 1), as well as to analyze the recorded data in order to determine any geomorphological changes triggered by this high-energy event. The morphosedimentary record of the AD 1755 tsunami in the Spanish and Portuguese coasts has been used as a comparative tool for the ancient tsunami (218–209 BC) documented in this study.

## 2. Study area

Doñana National Park is one of the largest wetlands (~500 km$^2$) in Europe, located in southwestern Spain (Fig. 1) where the Guadalquivir River is partly blocked in the lower reach by sandy spit-barriers, resulting in a large estuary (1800 km$^2$). This area is composed mainly of salt and freshwater marshes that include temporary ponds and have a modest topographic gradient (0–1 m). These marshes are drained by several tributaries and numerous ebb tide channels, with recent and ancient banks defined by clayey levees, bioclastic and beach-like sandy ridges (Fig. 1: Las Nuevas). In addition, these marginal formations are locally covered by sandy ridges aligned in an NE–SW orientation nearby to the Doñana spit-barrier (Fig. 1: Vetalengua). These inner zones are partly protected by two littoral spit-barrier system (Fig. 1: Doñana and La Algaida; 0–30 m height) composed of active dunes assembled in narrow (<100 m) and elongated (1–2 km) sandy strips.

In the regional Mediterranean littoral-barrier progradation, six morphosedimentary units ($H_{1-6}$) have been distinguished in southern Spain, separated by erosional events (Goy et al., 2003; Zazo, 2006). These units occur in this coast as former barrier islands separating lagoon systems from the sea. In the regional Atlantic spit-bar progradation, the morphosedimentary units ($H_{1-4}$) are less well-defined and dated (Zazo et al., 1994; Rodríguez-Ramírez et al., 1996): $H_1$ 6900–4500 cal BP, $H_2$ 4200–2600 cal BP, $H_3$ 2300–1100 cal BP, and $H_4$ 1000 cal BP to the Present. They represent the subaerial record of the Holocene coastal formations which, in the Atlantic–Mediterranean linkage area, began ca. 7000–6500 cal BP (Zazo et al., 1994; Dabrio et al., 2000).

The main hydrodynamic processes within the present estuary are controlled by the fluvial regime, tidal inputs, the dominant southwesterly wave action, and the southeasterly drift currents. The Guadalquivir River has a very irregular hydraulic regime, with a mean annual discharge of 185 m$^3$ s$^{-1}$ and maxima to 1000 m$^3$ h$^{-1}$ (Vanney, 1970). The tidal regime is mesotidal (mean range 2.15 m) and semidiurnal with a low diurnal inequality (Borrego et al., 1993). The maximum spring tidal range reaches 3.7 m.

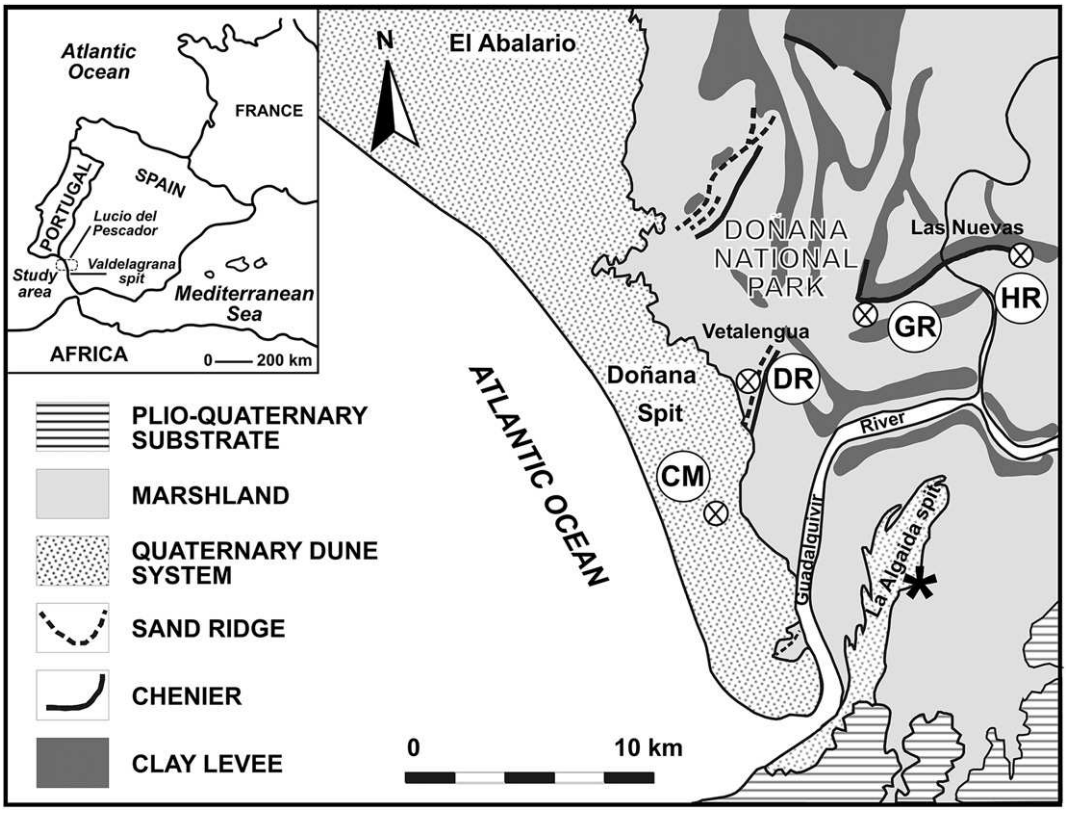


**Fig. 1.** Geographical location of the study area. Holocene morphosedimentary features and core sites (CM, DR, GR, HR) in the Guadalquivir estuary (Doñana marshlands). Star is the site of Fig. 5.

## 3. Materials and methods

### 3.1. Textural, mineralogical and palaeontological analyses

One long core (Fig. 1: CM (Corral de la Marta), ~7 m a.s.l., 31 m length) was collected by the Geological Survey of Spain (IGME) in the southern part of the Doñana marshlands. Additional samples to those obtained by Ruiz et al. (2004) were extracted from the uppermost part of three short cores collected in the same area (DR, GR and HR in Fig. 1).

Grain-size distribution was determined by wet sieving for the coarser fractions (>100 μm). Fractions lesser than 100 μm were analysed by photosedimentation (MicromeriticsR Sedigraph 5100 ET). Na-hexametaphosphate was used as a dispersing agent.

The mineralogical analysis of samples was carried out by means of X-ray diffraction (XRD) using a Siemens D-5000 equipment with a scanning speed of 1°2$\theta$/min and Cu-k$\alpha$ radiation. XRD studies were performed both on randomly oriented samples (total fraction) and clay fraction samples (<2 μm), the last prepared from cation-saturated, ultrasonic treated suspensions oriented on glass slides. The identification of the clay fraction minerals was carried out on oriented $Mg^{2+}$-saturated samples with ethylene glycol solution, after heating at 550 °C following $K^{+}$ saturation. When required, carbonates were eliminated using 0.6 N acetic acid. Quantitative estimation of the mineral content was carried out using the intensity factors calculated by Schultz (1964) and Barahona (1974).

In addition, the >63 μm fraction was studied under a stereoscopic microscope, in order to effectuate a general revision of the palaeontological record. This included the taxonomical determination and the estimation of both densities and diversities of bivalves, gastropods, ostracods and foraminifera. In addition, the presence and relative abundance of other groups (scaphopods, barnacles, bryozoans, crabs) were also noted.

### 3.2. Geomorphological mapping

The first geomorphological mapping of the Doñana marshlands were made and synthetically published in Rodríguez-Ramírez et al. (1996). Other maps of the Doñana area have been prepared later, focused on particular aspects, as is the case of the one developed in this study for the specific historical period (~220 BC–100 AD) (Fig. 6).

The survey made in this work is based on photointerpretations, along with field research, performed on bird-eye pictures taken in 1956 (1:33,000) and 1980 (1:10,000), satellite images of Google Earth and digital orthophotos of Andalucia (1:50,000). The Topographic Map of Andalucia (1:10,000) has been used as a base document for geomorphological mapping.

### 3.3. Radiocarbon chronology

Reliable radiocarbon dating of marine samples is hard to carry out since the initial specific $^{14}C$ activity differs from that of the contemporaneous atmosphere. The remaining $^{14}C$ activity of samples formed in the ocean reservoir not only reflects $^{14}C$ decay (related to sample age) but also the $^{14}C$ activity of the oceanic region where the sample lived (Stuiver and Braziunas, 1993). A correction for the age anomaly is possible when the reservoir–atmosphere offset in specific $^{14}C$ activity is known. The offset $R(t)$ is expressed as a reservoir $^{14}C$ age, which is not constant with time.

Secular $^{14}C$ variations in the marine environment can be represented by a modelled world ocean curve, but a world average curve does not account for regional oceanic differences in specific $^{14}C$ activity. Regional differences in $^{14}C$ content between the sea surface water for a specific region and the average surface water ones are due to several causes and anomalies, namely the upwelling of deep water. Thus, a parameter, denoted as $\Delta R$, can be defined as the difference between the reservoir age of the mixed layer of the regional ocean and the reservoir age of the mixed layer of the average world ocean (Stuiver and Braziunas, 1993).

A recent study concerning the reservoir effect in the coastal waters off the Gulf of Cádiz suggests a significant fluctuation with time in $\Delta R$ values during the Holocene (Soares and Dias, 2006). The computed weighted mean for $\Delta R$ is of $-135 \pm 20$ $^{14}C$ y in the Andalusian coast. Nevertheless, for the time interval 4400–4000 BP, $\Delta R$ values are strongly positive and in a first approach, between 4000 BP and 2500 BP, a $\Delta R$ value of $100 \pm 100$ $^{14}C$ y can be accepted (Soares and Martins, 2010). In the present work, the dates from various laboratories by radiocarbon analysis of mollusc shells (beach ridge, sand sheet) and peaty sand (marsh, dune), were obtained from selected previous papers and new sampling (Table 1).

The total dataset has fifteen radiocarbon dates that were converted into calendar dates using IntCal09 and Marine09 calibration curves (Reimer et al., 2009) for terrestrial and marine samples, respectively, and the program OxCal (Bronk Ramsey, 2001), version 4.1.3 (http://c14.arch.ox.ac.uk/oxcal.html). The final results are presented as calibrated ages for 2$\sigma$ intervals using a bayesian model (Fig. 2). The marine reservoir correction was carried out using a value of $-135 \pm 20$ $^{14}C$ y for $\Delta R$, with an exception for the date UtC-4031 (2930 ± 60 BP), which was calibrated using $\Delta R = 100 \pm 100$ $^{14}C$ y (Soares and Martins, 2010; Rodríguez-Vidal et al., 2010). Ages discussed below represent the highest probable age of the 2$\sigma$ calibrated range.

## 4. Results

### 4.1. Facies and palaeoenvironmental interpretation

The depth of cores DR, GR, and HR below ground surface are 120 cm, 150 cm, and 160 cm, respectively (Fig. 3). The cores were collected with a 20 mm diameter vibracore reaching up to 1.6 m depth. The sedimentological and compositional analyses of the core samples collected and dated in the Doñana marshlands enable the differentiation of six main facies.

#### 4.1.1. Facies FA-1. Laminated clayey silt

This facies occupies the upper part of core GR. It consists mainly of clayey silt and clay, with up to 65% of sediments included in the 40 μm to 4 μm grain-size interval for most samples. These sediments show a fine parallel lamination, with alternation of greyish to greenish (colour 6/1; Munsell scale) and blackish (colour 4/1) layers. Phyllosilicates (>70%) are clearly dominant over calcite (10–20%), quartz (<13%) and feldspars (<5%). Smectites (>50% in most cases) are slightly dominant over illite, with subordinate kaolinite.

The microscopical analysis reveals the presence of numerous reddish, oxidized fragments of roots, scarce gyrogonites of characeans (*Chara* sp., *Nitella* sp.) and isolated fragments of undifferentiated bivalves. A freshwater ostracod assemblage (*Cyprinotus salinus*, *Cyprideis torosa*, *Ilyocypris gibba*, *Herpetocypris chevreuxi*, *Cypris bispinosa*) is very abundant in this facies.

*Interpretation*: The main features of FA-1 have been observed in temporary ponds and the surrounding freshwater reedswamp of the Doñana marshlands, with similar ostracod and characean assemblages (Ruiz et al., 1996; Santos et al., 2006). These ponds are very shallow (<1 m in most cases) and contain alkaline, fresh to oligohaline waters. Fine lamination indicates a quiet environment with cyclic sedimentation as suggested by the alternating colour shading, probably due to alternating dry and wet periods, pulses from small tributaries or changes in the distribution of the vegetation (Whittecar et al., 2001; Harter and Mitsch, 2003).

**Table 1**
Radiocarbon dataset from Doñana marshlands (Guadalquivir estuary) and Valdelagrana spit (Bay of Cádiz) sedimentary records.

| Location (reference) | Lab. code | $^{14}$C age (BP) | Calibrated date (2$\sigma$) (cal BC/cal AD) Unmodelled | Calibrated date (2$\sigma$) (cal BC/cal AD) Modelled |
|---|---|---|---|---|
| *Phase pre-tsunami* | | | | |
| Doñana field dune (Zazo et al., 1999) | UtC-3929[a] | 2760 ± 60 | 1050–800 cal BC | 990–790 cal BC |
| Doñana field dune (Zazo et al., 1999) | LGQ-758[a] | 2590 ± 120 | 980–400 cal BC | 920–420 cal BC |
| Lucio El Pescador (Lario, 1996; Dabrio et al., 2000) | UtC–4028[c] | 2490 ± 60 | 790–410 cal BC | 800–480 cal BC |
| Lucio El Pescador (Lario, 1996; Dabrio et al., 2000) | UtC-4031[b] | 2930 ± 60 | 890–340 cal BC | 850–390 cal BC |
| CM core (this paper) | Beta-228876[b] | 2830 ± 40 | 770–230 cal BC | 780–370 cal BC |
| *Phase tsunami* | | | | |
| La Algaida spit (Zazo et al., 1994) | Beta-88022[b] | 2487 ± 70 | 590–150 cal BC | 480–140 cal BC |
| Las Nuevas N2 core (Rodríguez-Ramírez and Yáñez-Camacho, 2008) | Beta-145202[b] | 2570 ± 70 | 470 cal BC to 140 cal AD | 390–40 cal BC |
| Valdelagrana spit (Luque et al., 2002) | GX-27986[b] | 2340 ± 40 | 340–50 cal BC | 340–70 cal BC |
| | | *Sum* | 540 cal BC to 60 cal AD | 420–50 cal BC |
| *Phase post-tsunami* | | | | |
| Las Nuevas HR core (Rodríguez-Ramírez et al., 1996) | R-2278[b] | 2284 ± 39 | 250 cal BC to 40 cal AD | 160 cal BC to 40 cal AD |
| Las Nuevas GR core (Ruiz et al., 2004) | Beta-145203[b] | 2140 ± 70 | 130 cal BC to 250 cal AD | 100 cal BC to 100 cal AD |
| La Algaida spit (Rodríguez-Ramírez et al., 1996) | R-2284[b] | 2233 ± 29 | 160 cal BC to 60 cal AD | 110 cal BC to 60 cal AD |
| Vetalengua DR core (Ruiz et al., 2004) | Beta-88016[b] | 2230 ± 60 | 210 cal BC to 130 cal AD | 120 cal BC to 70 cal AD |
| Vetalengua DR core (Ruiz et al., 2004) | R-2283[b] | 2171 ± 36 | 90 cal BC to 140 cal AD | 80 cal BC to 90 cal AD |
| Doñana spit (Zazo et al., 1994) | R-2205[b] | 2185 ± 50 | 150 cal BC to 140 cal AD | 100 cal BC to 80 cal AD |
| CM core (this paper) | Beta-228874[b] | 2170 ± 40 | 100 cal BC to 150 cal AD | 90 cal BC to 90 cal AD |
| | | *Sum* | 200 cal BC to 160 cal AD | 110 cal BC to 80 cal AD |

Radiocarbon Laboratory: (UtC) Van der Graaf, Utrecht, Netherlands, (LGQ) Laboratoire de Géologie du Quaternaire, Luminy, France, (R) CNR Roma, Italy, (Beta) Beta Analytic Inc., Miami, USA, (GX) Geochron Laboratory, USA.
[a] Sample material: peaty sand.
[b] Sample material: shell.
[c] Sample material: twigs.

#### 4.1.2. Facies FA-2. Greyish silt

This facies is widely represented in all cores and is made-up of silt and clay (silt: 55–70%; clay: 26–43%) with greyish to greenish colours (5Y 4/2). Up to 70% of sediment is comprised between 15 and 2 μm, with high percentages of fine and very fine silt. They are structureless or show a very weak lamination.

Phyllosilicates are the main mineral components (40–67%; mean 57%), although both quartz (mean 14%) and calcite (mean 22%) increase in relation to FA-1. Smectites (46–60%) are dominant over illite (33–42%), kaolinite (7–12%) and chlorite (<5%).

The palaeontological record includes low densities of a brackish ostracod assemblage (mainly *C. torosa*, *Loxoconcha elliptica*, *Leptocythere castanea*), salt marsh foraminifera (*Ammonia tepida*, *Jadammina macrescens*, *Haynesina germanica*, *Trochammina inflata*), scarce freshwater gastropods (*Melanopsis*) and undifferentiated fragments of stems and roots. Reworked specimens of planktonic foraminifera, spines of echinoderms, bryozoans and marine or brackish bivalves (*Cardium edule*, *Venerupis decussatus*) are frequent.

*Interpretation*: This facies has intermediate characteristics between FA-1 and FA-3. The microfossil assemblages are characteristic of brackish marshes or of the adjacent margins of a brackish lagoon. Tidal flows introduced marine faunas towards the inner lagoonal areas. Both mineralogical and palaeontological records are very similar to those observed in the inner lagoons of the nearby Mediterranean rim (Ruiz et al., 2006b).

#### 4.1.3. Facies FA-3. Green silt and clay

These deposits consist of greenish clayey silt or silty clay (10 YR 5/3), with up to 70% of sediment (dry weight) comprised between 30 μm and 1 μm and very low sand contents (<4%). This facies-type displays a fine parallel lamination, with well-defined coarse laminae (5–10 cm thick) and scarce evidence of bioturbation.

The bulk mineralogy is dominated by phyllosilicates (mean 51%), reaching usually up to 47%. Calcite (19–32%; mean 25%) and quartz (13–16%) have more homogeneous distributions than FA-2, although similar mean values. Smectites (mean 54%) are dominant over illite (mean 39%), kaolinite (mean 7%) and chlorite (mean < 5%).

The macrofauna is composed of brackish (mainly *C. edule*) and marine (*V. decussatus*, *Chamelea gallina*) bivalves, together with less frequent specimens of marine gastropods (*Rissoa*, *Hinia*). Ostracods (2–200 individuals/gram; *C. torosa*, *L. elliptica*, *L. castanea*) and foraminifera (10–1000 individuals/gram; *A. tepida*, *H. germanica*) are frequent to very abundant in these sediments. The reworked marine faunas of ostracods, planktonic foraminifera, spines of echinoderms, fragments of bryozoans or centric diatoms may be locally abundant, constituting the 20–40% of the palaeontological record.

*Interpretation*: The most representative species of both ostracods and foraminifera are well represented in brackish lagoons (salinity up to 15–20‰). In this area, the tidal renewal is conditioned by the dimensions of outlets that cross the external, elongated sandy spits (Marocco et al., 1996; Ruiz et al., 2006a). This marine influence is proved by the presence of reworked faunas derived from the adjacent infralittoral zone (Pérez Quintero, 1989; Ruiz et al., 1997).

#### 4.1.4. Facies FA-4. Yellow silt

This is off-white to pale yellow, sandy-clayey silt (colour 8/2 to 8/3), poorly sorted, with very low to moderate percentages of sand (4–20%). They display parallel lamination or absence of patent sedimentary structures in some intervals. These fine-grained sediments are characterized by moderate to high percentages of quartz (20–44%) and low to moderate phyllosilicate contents (15–35%), In addition, calcite exceeds 20% and feldspars can be significant (~20%) in the upper part of core CM. Smectite and illite show similar proportions (40–50%).

Macrofauna is abundant, with numerous valves and fragments of marine molluscs, including bivalves (*C. gallina*, *V. decussatus*, *Acanthocardia tuberculata*), gastropods (*Rissoa* spp., *Hinia reticulata*, *Lemintina arenaria*) and scaphopods (*Dentalium vulgare, Dentalium sexangulum*). Benthic marine foraminifera (50–300 individuals/gram; *Ammonia beccarii*, *Quiqueloculina* spp., *Elphidium crispum*)

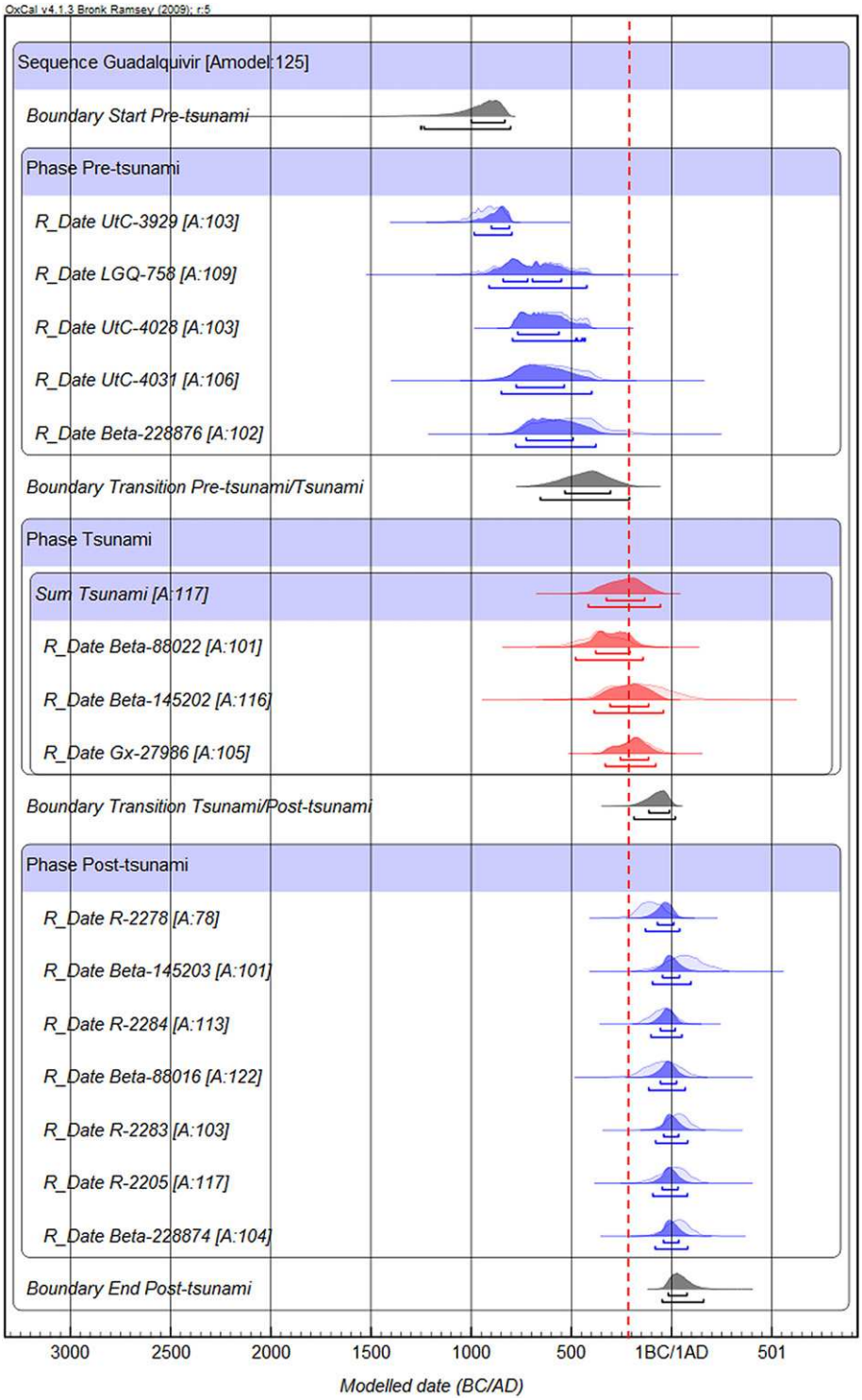


**Fig. 2.** Graphical representation of radiocarbon calibrated dataset generated by program OxCal. The broken line corresponds to the date of the 218–209 BC tsunami. A good agreement can be verified between the data and the OxCal model. Laboratory code in Table 1.

and ostracods (*Palmoconcha turbida*, *Pontocythere elongata*, *Urocythereis oblonga*) are dominant over brackish species. Fragments of bryozoans, plates of barnacles, claws of crabs, and planktonic foraminifera (*Orbulina*, *Globigerina*, *Globigerinoides*) are also abundant.

*Interpretation*: The most abundant assemblages of molluscs, ostracods and foraminifera of this facies characterize the shallow areas (<30 m depth) of the southwestern Spanish shelf (Pérez Quintero, 1989; Ruiz et al., 1997). These assemblages and some brackish specimens (*C. torosa*, *L. castanea*) are usually found in the marine zones of perimediterranean lagoons, very close to the natural or artificial inlets and subjected to moderate to high hydrodynamic gradients (Ruiz et al., 2006a, 2006b).

#### 4.1.5. Facies FA-5. Bioclastic silt and sand

This facies-type is the main component of several bioclastic beaches located at the margins of recent and ancient tidal channels

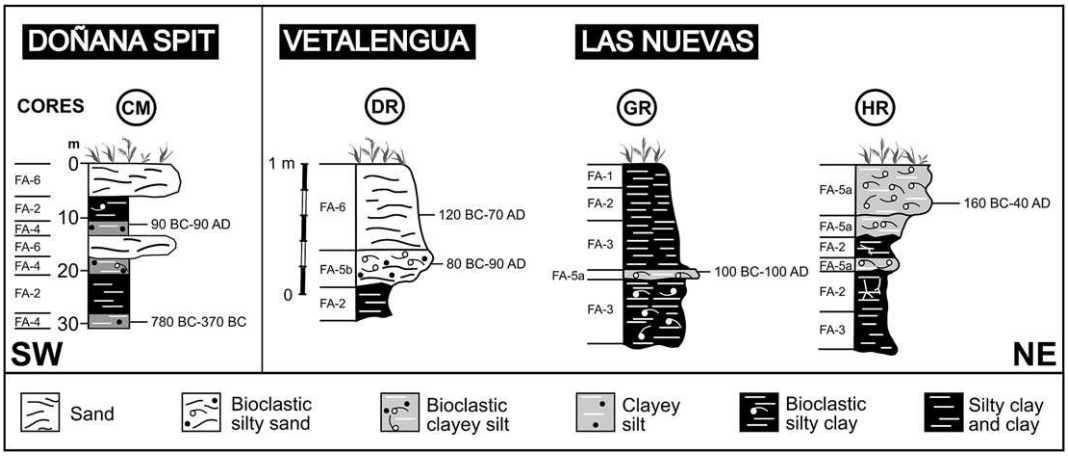


**Fig. 3.** Core profiles showing lithofacies and calibrated ages.

(Fig. 1: Las Nuevas). These sedimentary beds are characterized by a large lateral extension (3–6 km) and a narrow width (20–30 m). Thickness (5–70 cm in most cases) decreases landward, usually covering the FA-2 or FA-3 facies. They display an erosive base, with vegetation remains and intraclasts of the underlying sediments in the basal lag. In the upper part, bioclasts are in most cases fragmented and arranged in thick laminae (3–5 cm) or displaying a disorganized disposition. Textural analysis allows delimiting two subfacies, with a bimodal grain-size distribution and poor sorting in both cases.

*4.1.5.1. Subfacies FA-5-a.* Bioclasts are included in a greenish, clayey-silty matrix (5Y 8/3), with moderate sand contents (10–25%). Phyllosilicates (53–65%) are clearly dominant over calcite (mean 20%) and quartz (mean 12%). Illite is the main clay mineral (43–68%), with percentages slightly higher than smectites (28–47%), subordinated kaolinite (<5–15%) and chlorite (<5%) are also detected.

*4.1.5.2. Subfacies FA-5-b.* This subfacies is transitional to FA-6, with bioclasts included in a greenish to greyish silty-sandy matrix (5Y 8/6). In general, this facies exhibit fining-upward sequences, passing from basal fine sands to very fine sands with important contribution of silt near the top. Quartz is the main component (up to 70% in most cases), accompanied by secondary percentages of phyllosilicates (mean 11%) and feldspars (mean 10%). Illite ranges between 50% and 60% in all samples, with subordinated smectite (20–40%) and kaolinite (5–15%).

Molluscs represent an important proportion (10–40% dry weight) of the sediment. Shell debris and disarticulated bivalve shells of euryhaline (mainly *C. edule*) and marine (mainly *A. tuberculata*, *Donax vittatus* and *Spisula solida*) are abundant. Gastropods are represented by freshwater (*Gyraulus laevis*, *Melanopsis*) and marine (*Rissoa*, *Lemintina*, *Hinia*) specimens. Fragments of barnacles, scaphopods and bryozoans are also frequent.

Microfauna is better represented in subfacies FA-5-a, with 50–500 individuals/g of brackish ostracods (*C. torosa*, *L. elliptica*) and foraminifera (*A. tepida*, *H. germanica*), together with marine specimens of both groups (*Basslerites berchoni*, *Carinocythereis whitei*, *Urocythereis britannica*, *A. beccarii*, *E. crispum*). Some marine miliolids are also abundant (*Triloculina*, *Quinqueloculina*) lacking the last chambers in numerous individuals. Brackish ostracods present a high-energy population structure, with numerous individuals (>70% in most samples) corresponding to adults or A-1 to A-3 moults. On the contrary, only scarce specimens of brackish species were observed in the sandier samples of subfacies FA-5-b.

*Interpretation*: These ridges show numerous features described in tsunamigenic deposits (Bryant et al., 1992; Bryant, 2001; Dawson and Stewart, 2007): a) an erosional base; b) occurrence of intraclast and plant remains near the base; c) finer sediments towards the top; d) presence of higher sand percentages (near the Doñana spit-barrier) in relation to the underlying sediments; e) changes in the clay mineral composition; f) strong changes of fauna in relation to the underlying layers; g) presence of numerous marine species of both macrofauna and microfauna with evidence of reworking. Consequently, a tsunamigenic origin is attributed to these beds.

*4.1.6. Facies FA-6. Yellow sand*

This facies is represented in the uppermost part of Vetalengua and the dune system of Doñana spit-barrier (core CM). These layers consists of well sorted, fine to very fine sand with intense yellow shades (10Y 8/6). Up to 60% of sediment presents mean grain size comprised between 500 and 80 μm. In the upper levels of core CM, these sediments exhibit cross stratification, whereas they are massive in core DR. Both macrofauna and microfauna are virtually absent, with exception of some isolated and fragmented remains of the bivalve *Corbula gibba*.

Quartz (62–88%) is dominant over phyllosilicates (3–30%) and feldspars (5–21%). Smectites (54–56%) are the main clay minerals, with minor proportions of illite (34–40%) and kaolinite (6–10%).

*Interpretation*: These sediments constitute the dune system of the Doñana spit-barrier. The mineralogical records obtained coincide with those indicated by Flor (1990) in these aeolian materials.

*4.2. La Algaida high-energy facies*

The first eastern ridge of La Algaida spit-barrier (star in Fig. 1, and arrow in Fig. 4A) is a relict beach ridge of high-energy attached to a palaeocliff formed during the tsunami. The tsunami waves broke the previous tombolo and deposited a sedimentary formation composed of fine sands with numerous bioclasts, rock fragments and pebbles. These rock fragments (3–5 cm diameter) are quartz-rich sandstones and bioclastic calcarenites, rounded in some cases. They show shock marks, grooves and fractures filled by orange quartz-bearing sands, well sorted and slightly cemented with bioclast fragments. In addition, some incrusting organisms (bryozoans, annelids) are frequent in the surface of these pebbles and fragments.

*4.2.1. Macrofauna*

The matrix is almost azoic, with some occasional debris of bivalves (*Ostrea edulis*). Macrofauna is represented mainly by

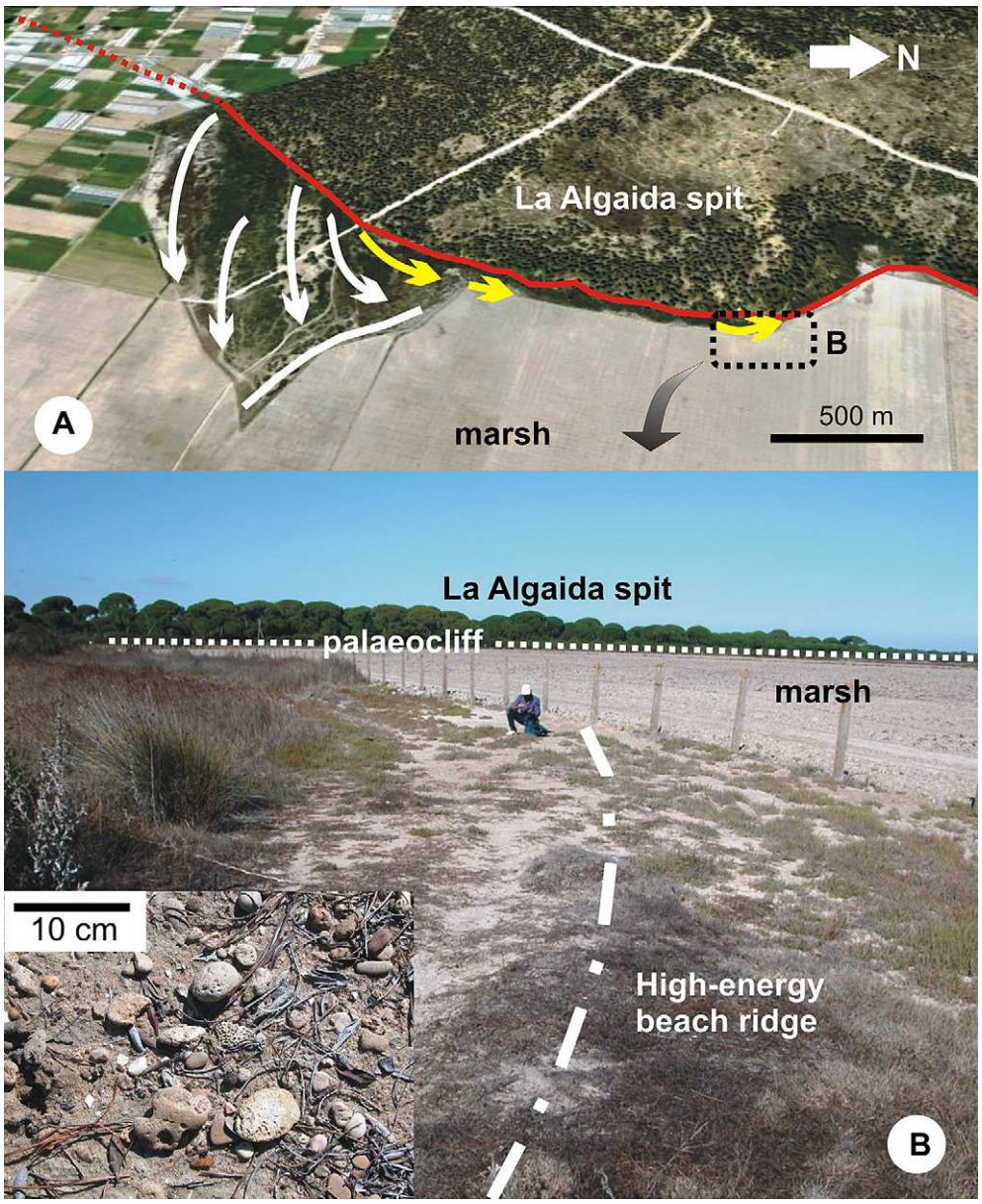


**Fig. 4.** La Algaida spit-barrier. A. Eastern shore with the tsunami beach ridge (yellow arrows; right hand side) and the post-tsunami ones (white arrows; left hand side), B. high-energy ridge attached to the former pre-tsunami palaeocliff and its sandy formation, with both rounded shells and bored clasts.

reworked molluscs. Rounded fragments of bivalves (*O. edulis*, *C. gallina*, *Glycymeris insubrica*, *Venus lamellosa*) are frequent, some of them highly bioeroded by clionid sponges (*Entobia*). Gastropods are abundant, with abundant evidence of transport (loss of the apex or the first whorls, abrasion of axial ornamentation, rupture of the outer lip or the aperture, shell fragmentation) in *Hexaplex trunculus*, *Conus mediterraneus*, *Cerithium vulgatum* or *Columbella rustica*.

*4.2.2. Microfauna*

The inner sediments of these mollusc shells show remarkable differences with the matrix. Foraminifera (mainly *A. beccarii*, *E. crispum*, *Quinqueloculina seminulum*, *A. tepida*) are abundant, with frequent losses of the last chambers in miliolids. In addition, fragments of planktic forms (e.g., *Orbulina universa*) have been also found. The ostracod population includes adults (*P. elongata*, *P. turbida*) and juvenile instars (*Loxoconcha rhomboidea*, *L. castanea*). Some isolated fragments of bryozoans, characeans and echinoderm spines complete the microfossil remains.

*4.2.3. Ichnology*

A high percentage of molluscs shows bioerosion evidence (*Caulostrepsis*, *Entobia*), most frequently in ostreids. In addition, some rare traces of *Oichnus paraboloides* Bromley have been found in naticids. Biotic boring activity has been also observed in numerous pebbles, with an ichnofabric dominated by eroded traces of *Entobia* sp. and small, poorly developed traces of *Cauloptrepsis* sp.

*4.2.4. Interpretation*

The sedimentological and palaeontological features of this ridge indicate a polygenetic geomorphological structure. The matrix is very similar to aeolian sediments of Doñana and La Algaida spit-barriers and the geomorphological beds derived from the erosion of them by tsunami or storm events (Ruiz et al., 2005). Contrast, the fossil record shows clear evidence of reworking, with the presence of transported specimens of marine species of ostracods (*P. elongata*, *P. turbida*), foraminifera (*A. beccarii*, *E. crispum*), bivalves (*G. insubrica*, *C. gallina*) or gastropods (*C. mediterraneus*, *C. rustica*).

At present, these species inhabit shallow to very shallow infralittoral environments in the adjacent Gulf of Cádiz (Pérez Quintero, 1989; Junta de Andalucía, 1993; Ruiz et al., 1997; Lindner, 2000). This marine origin is also contrasted by the occurrence of bryozoans, echinoderm remains or planktonic foraminifera.

Clasts show evidence of transport and shocks, indicating a high-energy original environment (shoreface–foreshore) with a continuous sedimentary reworking (Fig. 4B). They could come from former polygenic beaches of sands, bioclasts and pebbles located southward of the La Algaida spit-barrier. The provenance of the clasts can be only related with the erosion of Plio–Pleistocene cliffs (see the location of these materials in Fig. 1) with similar rocks (Domínguez et al., 2004; Del Río and Gracia, 2007).

## 5. Discussion

### 5.1. Geomorphological implication

Large tsunami produces significant geomorphological changes (Dawson, 1994; Fagherazzi and Du, 2008; Paris et al., 2009) when they reach the coast, including extensive erosion and deposition of different sedimentary layers. The direction of run-up flow on the coastal plain of Indonesia and Thailand (earthquake of December 26, 2004) was almost at 90° to the coastline, whereas backwash flow directions depended on topography (Umitsu et al., 2007). Coastal erosion of the plain was caused by the direct attack of tsunami waves, and the lower reaches of small rivers were eroded by a strong backwash flow. Intertidal areas are at present, exposed at low tide to the same extent as they were before the tsunami.

Thus, the main morphological changes undergone in the Indian Ocean and Andaman Sea coasts are shown by an erosive retreat of the shoreline, with generation of oblique channels, erosion of the sandy shoals and tip of littoral spits at the estuary mouth (Fagherazzi and Du, 2008; Pari et al., 2008), and deposition of sand sheets that penetrated several kilometres inland (Paris et al., 2007; Choowong et al., 2008), filling pre-existing furrows and making the terrain uniform (Hori et al., 2007). The great sedimentary load that penetrates up the estuaries will facilitate sedimentation as a basal residual lag or at the inner banks, either as a beach, ridge or washover fan (Narayana et al., 2007). Ebb tide delta and the regrowth of littoral spit-bar and barrier are frequent at an estuary mouth (Liew et al., 2010). Similarly, as observed in the New Zealand coastal dune systems (Goff et al., 2008), the tsunami inundation can modify existing dunes, producing features such as relict dune pedestals, landward sand sheets, hummocky topography, and parabolic dunes.

A similar model is proposed to have occurred in the Guadalquivir estuary during the tsunami of 218–209 BC. The great sand barrier of Doñana protected the coastal and tidal lowlands from erosion, although the first line of foredune and former dune ridges were eroded (Table 1: pre–420 cal BC). Accordingly, transgressive dunes were reactivated and migrated inland (Fig. 5). The sandy tip and shoals of the Doñana coastal-barrier were eroded suddenly, mainly by the backwash currents (Table 1: CM core 780–370 cal BC), as were the western and eastern flanks of the La Algaida spit-barrier. This created a channelled morphology, with small cliffs at right angles to the coastline, which are partially preserved today (Figs. 4 and 6B).

The sediments transported by the tsunami waves were spread over the estuary bed (Table 1: 420–50 cal BC) and subsequently accumulated at the edges of the marshes by tides and waves (Fig. 6B), forming the beach ridges of Vetalengua (Fig. 5), Las Nuevas, and La Algaida (Fig. 4), shaping the coastline of the ancient estuarine lagoon (*Lacus Ligustinus*) (Fig. 6C). These post-tsunami estuarine landscape has been dated (Table 1) between 110 cal BC–80 cal AD.

The growth of the Doñana and La Algaida spit-barriers continued with the episode of $H_3$ regional progradation (2300–1100 cal BP, Rodríguez-Ramírez et al., 1996), which sealed and fossilized the studied high-energy event (Table 2). Within the estuary, the sedimentation of marsh-type fine deposits continued.

### 5.2. Human settlement

This palaeogeographical and geomorphological reconstruction of the post-tsunami littoral landscape coincides with the earliest historical description of the estuary, made by the Roman chronicler Strabo in his work *Geographica*, written between 29 and 7 BC (Jones, 1917–1932). He referred to the southern part of the estuary as an inland lagoon (*Lacus Ligustinus*), a palaeogeography confirmed 40 years later by Mela, a Spanish chronicler, in his work *De Chorographica* (García Bellido, 1987).

The spit-barrier of La Algaida, on the eastern bank of the estuary, records the unique pre-Roman settlement (sanctuary, in Fig. 6A) documented in this coastal area (7th–3rd centuries BC: Blanco and Corzo, 1983). This ancient settlement was abandoned approximately at the date of the tsunami, when this sandy barrier was converted into an island (Rodríguez-Ramírez et al., 1996). Later, in the 1st

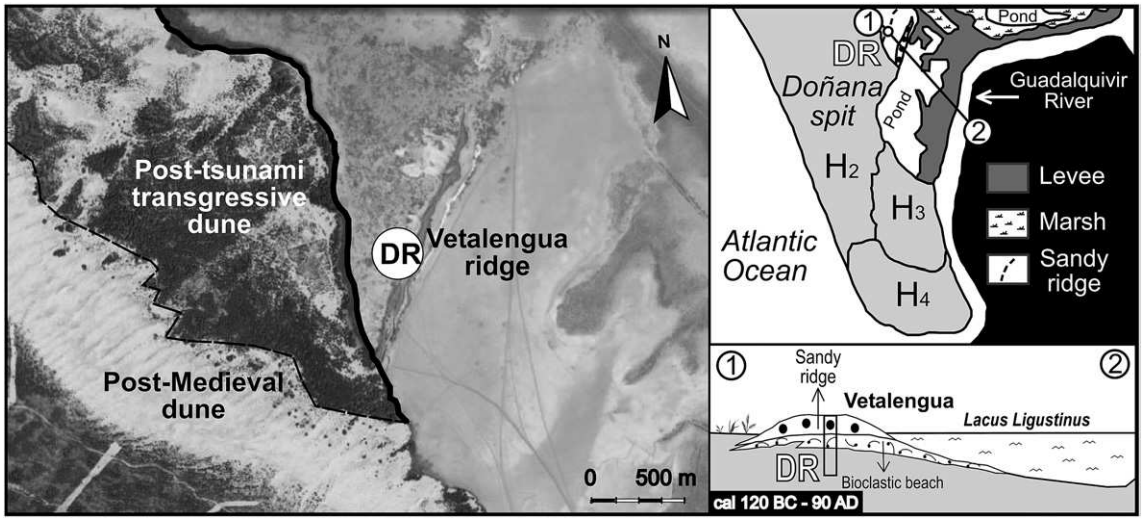


**Fig. 5.** Morphosedimentary formations of Vetalengua area and DR core. 1–2, interpretative cross-section of Vetalengua ridge during Roman time.

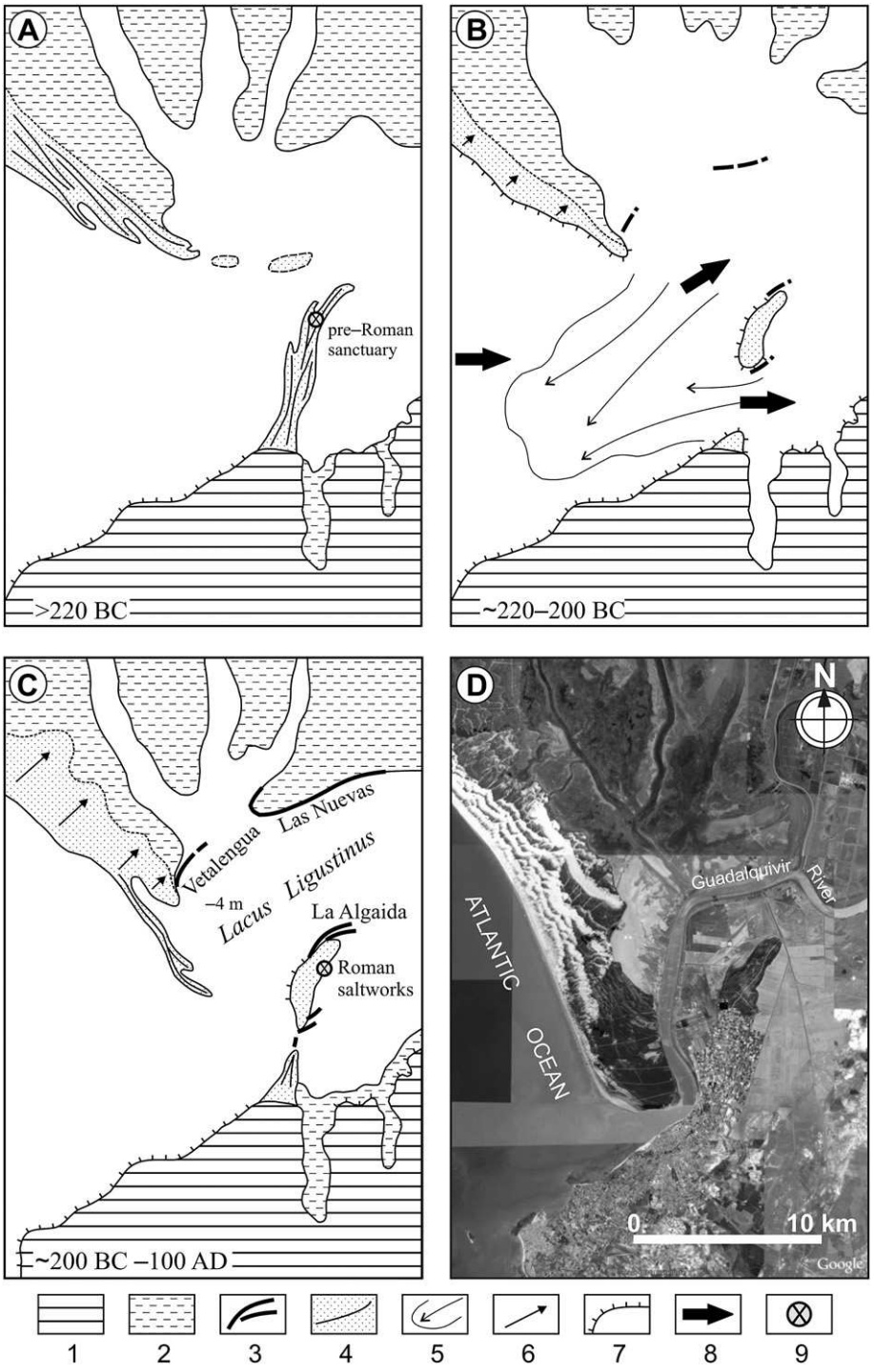


**Fig. 6.** Morphosedimentary evolution of the Guadalquivir estuary. A. pre-tsunami landscape (~220 BC), B. tsunami signatures and the landscape a few years later (~200 BC), C. post-tsunami *Lacus Ligustinus* (200 BC to 100 AD), D. present-day picture (Google Earth). Legend: 1. pre-Holocene substrate, 2. marshland, 3. beach ridge, 4. sandy formations and spit-ridge, 5. ebb tide delta, 6. transgressive dune, 7. cliff, 8. incoming tsunami, 9. human settlement.

century AD (Esteve Guerrero, 1952), and when the connection with the continent was re-established, the Romans installed a saltworks on the eastern coast, protected from wave action (Fig. 6C).

The chronological data coming from the shells of the tsunamigenic sediments and from the subsequent post-tsunami littoral sediments (phase post-tsunami, in Fig. 2), match the dates at which the historical descriptions were made by Strabo and Mela. The development of the post-tsunami landscape that was defined by a coastline of sandy beaches at the inner part of the estuary, happened between ~200 BC and 100 AD (Fig. 6C), ending up with a wide estuarine lagoon at its entrance. This was the *Lacus Ligustinus* that the Romans knew for 200 years approximately, between the 1st century BC and 1st century AD.

### 5.3. Morphosedimentary evolution

The morphosedimentary study of the current Guadalquivir estuary allows definition of an important tsunamigenic event,

**Table 2**
Re-calibrated radiocarbon dataset from Doñana and La Algaida spit-barriers (Guadalquivir estuary) and its correlation with regional progradation episode (after Rodríguez-Ramírez et al., 1996).

| Lab. code | $^{14}$C age (BP) | Calibrated date | | | | Regional progradation episode[a] |
|---|---|---|---|---|---|---|
| | | cal BC/cal AD | | cal BP | | |
| | | 1σ | 2σ | 1σ | 2σ | |
| Beta-88022[b] | 2487 ± 70 | 440–220 BC | 590–150 BC | 2390–2170 | 2540–2100 | H-2/H-3 (tsunami[c]) |
| R-2284[a] | 2233 ± 29 | 100 BC–20 AD | 160 BC–60 AD | 2050–1930 | 2110–1890 | H-3 |
| R-2272[a] | 1972 ± 40 | 190–340 AD | 130–390 AD | 1760–1610 | 1820–1560 | H-3 |
| R-2262[a] | 1865 ± 35 | 330–450 AD | 260–510 AD | 1620–1500 | 1690–1440 | H-3 |
| | | 380–520 AD | 320–580 AD | 1570–1430 | 1630–1370 | H-3/H-4 (erosion)[c] |
| R-2263[a] | 1800 ± 40 | 410–540 AD | 340–590 AD | 1540–1410 | 1610–1360 | H-4[c] |
| Beta-88018[b] | 1600 ± 60 | 600–730 AD | 530–810 AD | 1350–1220 | 1420–1140 | H-4[c] |
| Beta-88021[b] | 1530 ± 70 | 650–810 AD | 590–900 AD | 1300–1140 | 1360–1050 | H-4[c] |
| Beta-88020[b] | 1450 ± 70 | 720–890 AD | 670–980 AD | 1230–1060 | 1280–970 | H-4[c] |
| Beta-88019[b] | 1340 ± 60 | 850–1010 AD | 770–1060 AD | 1100–940 | 1180–890 | H-4[c] |

[a] Rodríguez-Ramírez et al., 1996.
[b] Zazo et al., 1994.
[c] This work.

related with one great submarine earthquake in the late 3rd century BC (218–209 BC) in the seismotectonic area of the Gulf of Cádiz (Campos, 1991). Particle-size analyses in this area also identified the occurrence of a high-energy event during Roman times (Lario et al., 2001; Luque et al., 2001). Similarly, other studies also identified a tsunami event in the Bay of Cádiz area for a broadly defined time-period of ca. 2000–2300 cal. BP (Luque et al., 2002), which probably corresponds to the event studied here.

The former Guadalquivir estuary had an obvious marine influence (Fig. 6A), as the Doñana spit-barrier was not as large as the present one and the estuary mouth was 8 km wide and 5–10 m in depth, according to the ostracod assemblage. The beach ridges of Vetalengua and Las Nuevas did not exist at that time, and this is why the inner part of the estuary was about 10 km to the north and almost 20 km wide from west to east-based on the former palaeogeographic reconstructions of Lario (1996), Rodríguez-Ramírez et al. (1996), Ruiz et al. (2004, 2005), and this work.

With all the data previously presented, it is possible to distinguish three evolutionary phases of the Guadalquivir palaeoestuary:

i) *Pre-tsunami phase* (Fig. 6A). During this phase, the continuous growth of the Doñana spit-barrier and the progressive infilling induced the formation of new brackish marsh (facies FA-2) or the transition from marine to more restricted littoral environments (facies FA-4 to facies FA-2). This phase is related to the later time of regional episode H-2 of coastal progradation (Table 2).
ii) *Tsunami phase* (Fig. 6B). A great tsunami eroded both the Doñana and La Algaida spit-barriers, introducing sandy sediment with shells (facies FA-5b of beach and FA-6 of dune) and rounded clasts towards the inner part of the estuary. The subtidal environments of the central part were buried by a sheet of bioclastic, silty-sandy sediments (facies FA-5a, core GR). The modelled age (2σ) of these sediments is 420–50 cal BC (Table 1 and Fig. 2).
iii) *Post-tsunami phase* (Fig. 6C). The first period of this phase was characterized by the accumulation of bioclastic sediments over the lagoon margins (facies FA-5, cores DR, GR, HR), wind-blown sand facies (FA-6, core DR), and an increasing infilling of the lagoon (cores GR and CM), with a progressive transition towards intertidal–supratidal conditions. This phase is related to the beginning of regional episode H-3 of coastal progradation (Table 2).

The subsequent palaeoenvironmental evolution of the Doñana marshlands (Fig. 6D) was controlled by the generation of new wetlands with temporary ponds (core GR) and the growing of the Doñana and La Algaida spit-barriers, with aeolian sands burying intertidal sediments (core CM). Regional sedimentary evidence of this tsunami include mineralogical indicators in the Guadalquivir estuary (Lario et al., 2001), the abrupt development of washover fans in the Guadalete estuary (Luque et al., 2002), rupture of the Punta Umbría spit-barrier (Rodríguez-Vidal, 1987), occurrence of large boulders and gravelly sands at +4 to +15 m a.s.l. near Lisbon (Scheffers and Kelletat, 2005), and a new turbiditic layer in the offshore SW Portuguese coast (Vizcaino et al., 2006).

The morphological and sedimentological changes in the coast triggered by this event were similar to (or even greater) than those related to the AD 1755 Lisbon tsunami event, probably because about that time the Gulf of Cádiz estuaries were still poorly protected by coastal barriers (Rodríguez-Ramírez et al., 1996), and tsunami waves could penetrate many kilometres deep inside, flooding the coeval inner lagoons and tidal plains. Comparison of the run-up of the AD 1755 tsunami in this area (Blanc, 2008; Lima et al., 2010) with that which must have happened during the 218–209 BC tsunami implies a flood height of at least 5 m a.s.l.

## 6. Conclusions

The morphosedimentary record of the pre-Roman and Roman evolution of the Guadalquivir River estuary allowed reconstruction of its main palaeogeographic features and demonstrated the occurrence of a very high-energy tsunamigenic event. The dating of the relocated sediments and the resulting erosive landform assemblage correlated it with the historically documented tsunami that occurred in the Atlantic Iberian coast between 218 and 209 BC (Campos, 1991).

The pre-tsunami estuarine lagoon was closed by two littoral spit-bars of almost similar dimensions (Doñana and La Algaida) with sandy shoals and a mouth width of 8 km. The estuary had a well-developed muddy tidal flat, and the lagoon had a dimension of about 10 km to the north and 20 km approximately from west to east.

The tsunami we recorded in this estuary had probably a similar or greater magnitude ($M_w \geq 8.5$) than the AD 1755 event, also recorded in this coast. The erosion of the tsunamigenic waves focused in the littoral spits, in which morphological evidence remains, including cliffs and incisions. The spit-barrier of La Algaida became an island, and the human settlements were abandoned. After that, the eroded foredunes migrated inland, in the form of transgressive blown sand sheets. The bioclastic sand, brought into the estuary, was accumulated in the lagoon margins, leading the development of the estuarine sandy ridges of Vetalengua and Las Nuevas.

The reorganization of the relocated sediments by the tsunami and their accumulation at the sides of the Guadalquivir estuary formed the sand ridges of Doñana, Vetalengua, Las Nuevas and La Algaida, placed over sand shoal or previous bioclastic sand and silt. The tsunami action, the consequent relocation of sediments and morphological changes triggered within the ancient estuary, controlled the palaeogeography of the *Lacus Ligustinus* during the early Roman times in southern Spain.

## Acknowledgements

This research was funded by the Spanish–FEDER Projects CTM2006–06722/MAR, CGL2006–01412/BTE and CGL2010–15810/BTE, and three Research Groups of the Andalusia Board (RNM–238, RNM–293, and RNM–349). We thank reviewers and guest-editors for helpful comments. Darren Fa improved the English of the manuscript. This work is a contribution to the IGCPs 526 (Risks, resources, and record of the past on the continental shelf), 567 (Earthquake Archaeology and Palaeoseismology), and 588 (Preparing for coastal change).

## References

Alexander, D., 1993. Natural Disasters. ULC Press, London, 632 pp.
Babu, N., Suresh Babu, D.S., Mohan Das, P.N., 2007. Impact of tsunami on texture and mineralogy of a major placer deposit in southwest coast of India. Environmental Geology 52, 71–80.
Baptista, M.A., Heitor, S., Miranda, J.M., Miranda, P., Mendes Victor, L., 1998. The 1755 Lisbon tsunami; evaluation of the tsunami parameters. Journal of Geodynamics 25, 143–157.
Barahona, E., 1974. Arcillas de ladrillería de la provincia de Granada: evaluación de algunos ensayos de materias primas. Ph.D. Thesis. University of Granada, Spain.
Blanc, P.-L., 2008. The tsunami in Cadiz on 1 November 1755: a critical analysis of reports by Antonio de Ulloa and by Louis Godin. Comptes Rendus Geoscience 340, 251–261.
Blanco, A., Corzo, R., 1983. Monte Algaida. un santuario púnico en la desembocadura del Guadalquivir. Historia-16 87, 122–128.
Borrego, J., Morales, J.A., Pendón, J.G., 1993. Holocene filling of an estuarine lagoon along the mesotidal coast of Huelva: the Piedras River mouth, southwestern Spain. Journal of Coastal Research 8, 321–343.
Borrego, J., López González, N., Carro, B., 2004. Geochemical signature as palaeoenvironmental markers in Holocene sediments of the Tinto River estuary (Southwestern Spain). Estuarine, Coastal and Shelf Science 61, 631–641.
Borrero, J.C., 2005. Field data and satellite imagery of tsunami effects in Banda Aceh. Science 308, 1596.
Bronk Ramsey, C., 2001. Development of the radiocarbon calibration program OxCal. Radiocarbon 43 (2A), 355–363.
Bryant, E.A., 2001. Natural Hazards. Cambridge University Press, Hong Kong.
Bryant, E.A., Young, R.W., Price, D.M., 1992. Evidence of tsunami sedimentation on the southeastern coast of Australia. Journal of Geology 100, 753–765.
Campos, M.L., 1991. Tsunami hazard on the Spanish coasts of the Iberian Peninsula. Science of Tsunami Hazards 9, 83–90.
Carretero, M.I., Ruiz, F., Rodríguez Ramírez, A., Cáceres, L.M., Rodríguez-Vidal, J., González-Regalado, M.L., 2002. The use of clay minerals and microfossils in palaeoenvironmental reconstructions: the Holocene littoral strand of Las Nuevas (Doñana National Park, SW Spain). Clay Minerals 37, 93–103.
Chamley, H., 1989. Clay Sedimentology. Springer Verlag, Berlin.
Choowong, M., Murakoshi, N., Hisada, K., Charoentitirat, T., Charusiri, P., Phantuwongraj, S., Wongkok, P., Choowong, A., Subsayjun, R., Chutakositkanon, V., Jankaew, K., Kanjanapayont, P., 2008. Flow conditions of the 2004 Indian Ocean tsunami in Thailand inferred from capping bedforms and sedimentary structures. Terra Nova 20, 141–149.
Clague, J.J., Bobrowsky, P.T., Hutchinson, I., 2000. A review of geological records of large tsunami at Vancouver Island, British Columbia. Quaternary Science Reviews 19, 849–863.
Dabrio, C.J., Zazo, C., Lario, J., Goy, J.L., Sierro, F.J., Borja, F., et al., 2000. Depositional history of estuarine infill during the last postglacial transgression (Gulf of Cadiz, southern Spain). Marine Geology 162, 381–404.
Dawson, A.G., 1994. Geomorphological effects of tsunami run-up and backwash. Geomorphology 10, 83–94.
Dawson, A.G., Stewart, I., 2007. Tsunami deposits in the geological record. Sedimentary Geology 200, 166–183.
Del Río, L., Gracia, F.J., 2007. Análisis de la vulnerabilidad de los acantilados atlánticos de la provincia de Cádiz ante la erosión costera. Cuaternario y Geomorfología 21, 87–101.
Domínguez, L., Gracia, F.J., Anfuso, G., 2004. Tasas de avance/retroceso de la línea de costa mediante morfometría fotogravimétrica en el sector Sanlúcar de Barrameda-Rota (provincia de Cádiz). Revista de la Sociedad Geológica de España 17, 71–86.
Esteve Guerrero, M., 1952. Sanlúcar de Barrameda (Cádiz): fábrica de salazón romana en la Algaida. Noticiario Arqueológico Hispánico 1–3, 126–133.
Fagherazzi, S., Du, X., 2008. Tsunamigenic incisions produced by the December 2004 earthquake along the coasts of Thailand, Indonesia and Sri Lanka. Geomorphology 99, 120–129.
Flor, G., 1990. Tipología de dunas eólicas. procesos de erosión, sedimentación costera y evolución litoral de la provincia de Huelva (Golfo de Cádiz occidental, Sur de España). Estudios Geológicos 46, 99–109.
Galbis, R.J., 1932. Catálogo sísmico de la zona comprendida entre los meridianos 58° E y 20° W de Greenwich y los paralelos 45° y 25° N. Dirección General del Instituto Geográfico, Catastral y de Estadística, Madrid.
García Bellido, A., 1987. La España del siglo primero de nuestra era (según P. Mela y C. Plinio). Colección Austral, Espasa Calpe.
Goff, J., McFadgen, B., Wells, A., Hicks, M., 2008. Seismic signals in coastal dune systems. Earth-Science Reviews 89, 73–77.
Goy, J.L., Zazo, C., Dabrio, C.J., 2003. A beach-ridge progradation complex reflecting periodical sea-level and climate variability during the Holocene (Gulf of Almería, Western Mediterranean). Geomorphology 50, 251–268.
Harter, S.K., Mitsch, W.J., 2003. Patterns of short-term sedimentation in a freshwater created marsh. Journal of Environmental Quality 32, 325–334.
Hori, K., Kuzumoto, R., Hirouchi, D., Umitsu, M., Janjirawuttikul, N., Patanakanog, B., 2007. Horizontal and vertical variation of 2004 Indian tsunami deposits: an example of two transects along the western coast of Thailand. Marine Geology 239, 163–172.
Jones, H.L. (Ed.), 1917–1932. The Geography of Strabo. Harvard University Press and Heinemann.
Junta de Andalucía, 1993. Atlas de los recursos marinos del Golfo de Cádiz. In: de Huelva, Litoral (Ed.). Junta de Andalucía, España, p. 145.
Lario, J., 1996. Último y Presente Interglacial en el área de conexión Atlántico – Mediterráneo: Variaciones del nivel del mar, paleoclima y paleoambientes. Unpublished Ph.D. Thesis. Universidad Complutense de Madrid, 269p.
Lario, J., Zazo, C., Plater, A.J., Goy, J.L., Dabrio, C., Borja, F., et al., 2001. Particle size and magnetic properties of Holocene estuarine deposits from the Doñana National Park (SW Iberia): evidence of gradual and abrupt coastal sedimentation. Zeitschrift für Geomorphologie 45, 33–45.
Liew, S.C., Gupta, A., Wong, P.P., Kwoh, L.K., Lindner, G., 2010. Recovery from a large tsunami mapped over time: the Aceh coast, Sumatra. Geomorphology 114, 520–529.
Lima, V.V., Miranda, J.M., Baptista, M.A., Catalão, J., Gonzalez, M., Otero, L., et al., 2010. Impact of a 1755-like tsunami in Huelva, Spain. Natural Hazards and Earth System Sciences 10, 139–148.
Lindner, G., 2000. Moluscos y caracoles de los mares del mundo. Ediciones Omega, Barcelona, 319 pp.
Luque, L., Lario, J., Zazo, C., Goy, J.L., Dabrio, C.J., Silva, P.G., 2001. Tsunami deposits as palaeoseismic indicators: examples from the Spanish coast. Acta Geológica Hispánica 3–4, 197–211.
Luque, L., Lario, J., Civis, J., Silva, P.G., Zazo, C., Goy, J.L., Dabrio, C.J., 2002. Sedimentary record of a tsunami during Roman times, Bay of Cadiz, Spain. Journal of Quaternary Science 17, 613–631.
Mackie, E.A.V., Lloyd, J.M., Leng, M.J., Bentley, M.J., Arrowsmith, C., 2007. Assessment of $\delta^{13}C$ and C/N ratios in bulk organic matter as palaeosalinity indicators in Holocene and Lateglacial isolation basin sediments, northwest Scotland. Journal of Quaternary Science 22, 579–591.
Marocco, R., Melis, R., Montenegro, M.E., Pugliese, N., Vio, E., Lenardon, G., 1996. Holocene evolution of the Caorle barrier lagoon (northern Adriatic Sea, Italy). Rivista Italiana di Paleontologia e Stratigrafia 102, 385–396.
Monecke, K., Finger, W., Klarer, D., Kongko, W., McAdoo, B.G., Moore, A.L., Sudrajat, S.U., 2008. A 1000-year sediment record of tsunami recurrence in northern Sumatra. Nature 455, 1232–1234.
Narayana, A.C., Tatavarti, R., Shinu, N., Subeer, A., 2007. Tsunami of December 26, 2004 on the southwest coast of India: post-tsunami geomorphic and sediment characteristics. Marine Geology 242, 155–168.
Pari, Y., Ramana Murthy, M.V., Jaya kumar, S., Subramanian, B.R., Ramachandran, S., 2008. Morphological changes at Vellar estuary, India – impact of the December 2004 tsunami. Journal of Environmental Management 89, 45–57.
Paris, R., Lavigne, F., Wassmer, P., Sartohadi, J., 2007. Coastal sedimentation associated with the December 26, 2004 tsunami in Lhok Nga, west Banda Aceh (Sumatra, Indonesia). Marine Geology 238, 93–106.
Paris, R., Wassmer, P., Sartohadi, J., Lavigne, F., Barthomeuf, B., Desgages, E., Grancher, D., Baumert, P., Vautier, F., Brunstein, D., Gomez, C., 2009. Tsunami as geomorphic crises: lessons from the December 26, 2004 tsunami in Lhok Nga, west Banda Aceh (Sumatra, Indonesia). Geomorphology 104, 59–72.
Pérez Quintero, J.C., 1989. Introducción a los Moluscos onubenses, I: Faunística. Junta de Andalucía, Spain.
Pozo, M., Ruiz, F., Carretero, M.I., Rodríguez-Vidal, J., Cáceres, L.M., Abad, M., González-Regalado, M.L., 2010. Mineralogical assemblages, geochemistry and fossil associations of Pleistocene–Holocene complex siliciclastic deposits from the Southwestern Doñana National Park (SW Spain): a palaeoenvironmental approach. Sedimentary Geology 225, 1–18.
Reicherter, K., 2001. Paleoseismological advances in the Granada Basin (Betic Cordilleras, southern Spain). Acta Geológica Hispánica 36, 267–281.
Reimer, P.J., Baillie, M.G.L., Bard, E., Bayliss, A., Beck, J.W., Blackwell, P.G., Bronk Ramsey, C., Buck, C.E., Burr, G.S., Edwards, R.L., Friedrich, M., Grootes, P.M., Guilderson, T.P., Hajdas, I., Heaton, T.J., Hogg, A.G., Hughen, K.A., Kaiser, K.F.,

Kromer, B., McCormac, F.G., Manning, S.W., Reimer, R.W., Richards, D.A., Southon, J.R., Talamo, S., Turney, C.S.M., van der Plicht, J., Weyhenmeyer, C.E., 2009. IntCal09 and Marine09 radiocarbon age calibration curves, 0–50,000 years cal BP. Radiocarbon 51 (4), 1111–1150.

Rodríguez-Ramírez, A., Rodríguez-Vidal, J., Cáceres, L.M., Clemente, L., Belluomini, G., Manfra, L., Improta, S., de Andrés, J.R., 1996. Recent coastal evolution of the Doñana National Park (SW Spain). Quaternary Science Reviews 15, 803–809.

Rodríguez-Ramírez, A., Yáñez-Camacho, C.M., 2008. Formation of chenier plain of the Doñana marshland (SW Spain): observations and geomorphic model. Marine Geology 254, 187–196.

Rodríguez-Vidal, J., 1987. Modelo de evolución geomorfológica de la flecha litoral de Punta Umbría, Huelva, España. Cuaternario y Geomorfología 1, 247–256.

Rodríguez-Vidal, J., Soares, A.M.M., Ruiz, F., Cáceres, L.M., 2010. Comment on "Formation of chenier plain of the Doñana marshland (SW Spain): observations and geomorphic model" by A. Rodríguez-Ramírez and C.M. Yáñez-Camacho [Marine Geology 254 (2008) 187–196]. Marine Geology 275, 292–295.

Ruiz, F., González-Regalado, M.L., Serrano, L., Toja, J., 1996. Los ostrácodos de las lagunas temporales del Parque Nacional de Doñana. Aestuaria 4, 125–140.

Ruiz, F., González-Regalado, M.L., Muñoz, J.M., 1997. Multivariate analysis applied to total and living fauna: seasonal ecology of recent benthic ostracoda off the North Cadiz Gulf Coast (SW Spain). Marine Micropaleontology 31, 183–203.

Ruiz, F., Rodríguez Ramírez, A., Cáceres, L.M., Rodríguez-Vidal, J., Carretero, M.I., Clemente, L., Muñoz, J.M., Yáñez, C., Abad, M., 2004. Late Holocene evolution of the southwestern Doñana National Park (Guadalquivir Estuary, SW Spain): a multivariate approach. Palaeogeography, Palaeoclimatology, Palaeoecology 204, 47–64.

Ruiz, F., Rodríguez Ramírez, A., Cáceres, L.M., Rodríguez-Vidal, J., Carretero, M.I., Abad, M., Olías, M., Pozo, M., 2005. Evidence of high-energy events in the geological record: mid-Holocene evolution of the southwestern Doñana National Park (SW Spain). Palaeogeography, Palaeoclimatology, Palaeoecology 229, 212–229.

Ruiz, F., Abad, M., Galán, E., González, I., Aguilá, I., Olías, M., Gómez Ariza, J.L., Cantano, M., 2006a. The present environmental scenario of El Melah Lagoon (NE Tunisia) and its evolution to a future sabkha. Journal of African Earth Science 44, 289–302.

Ruiz, F., Abad, M., Olías, M., Galán, E., González, I., Aguilá, E., Hamoumi, N., Pulido, I., Cantano, M., 2006b. The present environmental scenario of the Nador Lagoon (Morocco). Environmental Research 102, 215–229.

Santos, A., Sousa, A., Fernández, R., García, P., 2006. Aquatic macrophytes in Doñana protected area (SW Spain): an overview. Limnetica 25, 71–80.

Scheffers, A., Kelletat, D., 2005. Tsunami relics on the coastal landscape west of Lisbon, Portugal. Science of Tsunami Hazards 23, 3–16.

Schultz L.G., 1964. Quantitative interpretation of mineral composition from X-ray and chemical data for the Pierre Shale. United States Geological Survey Professional Paper 391C.

Selby, K.A., Smith, D.E., 2007. Late Devensian and Holocene sea-level changes on the Isle of Skye, Scotland, UK. Journal of Quaternary Science 22, 119–139.

Singarasubramanian, S.R., Mukesh, M.V., Manoharan, K., Murugan, S., Bakkiaraj, D., Meter, A.J., Seralathan, P., 2006. Sediment characteristics of the M-9 tsunami event between Rameswaram and Thoothukudi, Gulf of Mannar, southeast coast of India. Science of Tsunami Hazards 25, 160–172.

Soares, A.M.M., Dias, J.M.A., 2006. Once upon a time into the Azores Front penetrated into the Gulf of Cadiz. In: Abstracts 5th Symposium on the Iberian Atlantic Margin, 3pp.

Soares, A.M.M., Martins, J.M.M., 2010. Radiocarbon dating of marine samples from Gulf of Cadiz: the reservoir effect. Quaternary International 221, 9–12.

Solares, J.M.M., Arroyo, A.L., 2004. The great historical 1755 earthquake. Effects and damage in Spain. Journal of Seismology 8, 275–294.

Stuiver, M., Braziunas, T.F., 1993. Modeling atmospheric $^{14}C$ influences and $^{14}C$ ages of marine samples to 10,000 BC. Radiocarbon 35, 137–189.

Umitsu, M., Tanavud, C., Patanakanog, B., 2007. Effects of landforms on tsunami flow in the plains of Banda Aceh, Indonesia, and Nam Khem, Thailand. Marine Geology 242, 141–153.

Vanney, J.R., 1970. L'hydrologie du Bas Guadalquivir. CSIC-Consejo Superior de Investigaciones Científicas, Madrid.

Vilanova, I., Prieto, A.R., Espinosa, M., 2006. Palaeoenvironmental evolution and sea-level fluctuations along the southeastern Pampa grasslands coast of Argentina during the Holocene. Journal of Quaternary Science 21, 227–242.

Vizcaino, A., Gràcia, E., Escutia, C., Asioli, A., García-Orellana, J., Lebreiro, S., Cacho, I., Thouveny, N., Larrasoaña, J.C., Diez, S., Dañobeitia, J.J., 2006. Characterizing Holocene paleoseismic record in the SW Portuguese Margin. Geophysical Research Abstracts 8, 08469.

Whittecar, G.R., Megonigal, J.P., Darke, A.K., 2001. Sedimentation patterns within tidal fresh-water marshes, Mattaponi River, Virginia. In: GSA Annual meeting, Boston, session 180, booth 69.

Zazo, C., 2006. Cambio climático y nivel del mar: la península ibérica en el contexto global. Cuaternario y Geomorfología 20, 115–130.

Zazo, C., Goy, J.L., Somoza, L., Dabrio, C.J., Belluomini, G., Improta, S., Lario, J., Bardaji, T., Silva, P.G., 1994. Holocene sequence of sea-level fluctuations in relation to climatic trends in the Atlantic-Mediterranean linkage coast. Journal of Coastal Research 10, 933–945.

Zazo, C., Dabrio, C.J., Borja, F., Goy, J.L., Lezine, A.M., Lario, J., Polo, M.D., Hoyos, M., Boersma, J.R., 1999. Pleistocene and Holocene aeolian facies along the Huelva coast (southern Spain): climatic and neotectonic implications. Geologie en Mijnbouw 77, 209–224.